Study on effect of enhanced creep properties of T92 cladding on CDF for the steady-state condition in PGSFR using finite element analysis

Hyun-Woo Jung, Hyun-Kyu Song, Jin-Ha Hwang, Thanh-Long Nguyen, Yun-Jae Kim*
Dept. of Mechanical Engineering, Korea Univ., 5ga Anam-dong, Sungbuk-gu, Seoul, Korea
**Corresponding author: kimy0308@korea.ac.kr*

1. Introduction

In advanced Gen IV sodium fast reactors (SFR), fuel pins are expected to be irradiated by fast neutron at higher temperature than in previous reactors. The integrity of fuel pin is strongly dependent on the ability of the cladding to tolerate the harsh environment of SFR systems. The cladding material of SFR should be resistant to creep and irradiation, so that the cladding maintains low creep damage, low swelling and high ductility for its lifetime.

Ferric-martensitic (F-M) stainless steel is potential candidate of cladding material for SFR. HT9 is primary F-M steel adopted by the US fast reactor program. Similar F-M steels have been chosen in Japan and Europe. The prototype Gen IV sodium cooled fast reactor (PGSFR) in Korea also adopted HT9 as cladding material. These F-M steels have excellent swelling resistance but low creep strength at temperatures above 650 ºC desired in the SFR systems.

Several F-M steels have been developed to enhance their creep strength. T92 is one of creep-strength-enhanced F-M steel that has far better creep strength and irradiation resistance than primary F-M steels.

In this study, to quantify the effect of enhanced creep property of T92 cladding on reliability of fuel pin, the cumulative damage fraction (CDF) of T92 and HT9 claddings were evaluated and compared for the steady-state condition in PGSFR using finite element analysis. As the finite element (FE) analysis software, Abaqus 2016 was used.

2. Methods

3.1. Fuel pin model

The parameters of the fuel pin used in this study are suggested in Table I. Two dimensional axisymmetric 4-node elements, CAX4 and DCAX4 supported by Abaqus 2016 were used for structural and heat transfer analysis, respectively. FE analysis model is suggested in Fig. 1. Total 16,170 elements were used in the fuel pin model.

Table I: Fuel Pin Parameter

Fuel type	U-10Zr
Cladding material	HT9 / T92
Total length	2150 mm
Fuel slug length	900 mm
Fuel radius	2.77 mm
Cladding outer radius	3.7 mm
Cladding Inner radius	3.2 mm
Wire radius	0.475 mm

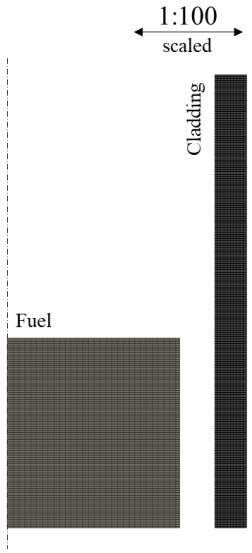

Fig. 1. FE analysis model of fuel pin

3.2. Material properties for FE analysis

Thermal conductivity of as-fabricated U-Zr fuel is suggested in following equation [1]:

$$k_0 = A + BT + CT^2$$
$$A = 17.5(1 - 2.23W_{Zr}) / (1 + 1.61W_{Zr})$$
$$B = 1.54 \times 10^{-2}(1 + 0.061W_{Zr}) / (1 + 1.61W_{Zr})$$
$$C = 9.38 \times 10^{-6} \quad (1)$$

k_0 is as-fabricated thermal conductivity of fuel in *W/m/K*, T is temperature in K, and W_{Zr} is zirconium weight fraction. Specific heat and density were obtained from regionwise interpolation result conducted by SAS4A SSCOMP [2].

Thermal conductivity of HT9 is given in following equation [3]:

$$k_c = \begin{cases} 17.622 + 2.42 \times 10^{-2} T - 1.696 \times 10^{-5} T^2 & (T < 1030) \\ 12.027 + 1.218 \times 10^{-2} T & (T \geq 1030) \end{cases} \quad (2)$$

k_c is thermal conductivity of HT9 in *W/m/K*, and T is temperature in *K*. Specific heat of HT9 is suggested in following equation [4]:

$$c_{pc} = \begin{cases} \frac{1}{6}(T - 500) + 500 & (T < 800) \\ \frac{3}{5}(T - 800) + 550 & (T \geq 800) \end{cases} \quad (3)$$

c_{pc} is specific heat of HT9 in *J/kg/K*, and T is temperature in *K*. It was assumed that T92 has same

thermal conductivity and specific heat as HT9. Assigned density of HT9 and T92 is 8000 kg/m^3.

Young's modulus and Poisson's ratio of HT9 are given in following equations [5]:

$$E_c = (213.28 - 4.799\times10^{-2}T - 4.065\times10^{-6}T^2)\times10^3 \quad (4)$$

$$\nu_c = 0.2762 + 8.9309\times10^{-5}T - 6.262\times10^{-8}T^2 \quad (5)$$

E_c is Young's modulus of HT9 in *MPa*, ν_c is Poisson's ratio of HT9, and T is temperature in ^oF. Thermal expansion strain of HT9 is suggested in following equation [3]:

$$\varepsilon_{tc} = -0.2191\times10^{-2} + 5.678\times10^{-6}T + 8.111\times10^{-9}T^2 - 2.576\times10^{-12}T^3 \quad (6)$$

ε_{tc} is thermal expansion strain, and T is temperature in K. It was assumed that T92 has same Young's modulus, Poisson's ratio and thermal expansion coefficient as HT9.

In this analysis, the only differences of mechanical property between HT9 and T92 were creep strain rate and creep rupture time to calculate CDF. Steady-state creep strain rate and creep rupture time of HT9 is suggested in following equations [2]:

$$\begin{aligned}
&\dot{\varepsilon}_{ss} = \dot{\varepsilon}_{oos}\left(\frac{E}{\sigma_{so}}\right)^n\left(\frac{\sigma_{eq}}{E}\right)^n \exp\left(-\frac{Q_c}{kT}\right)\\
&\dot{\varepsilon}_{oos} = 5.1966\times10^{10}\\
&\sigma_{so}/\mathrm{E} = 3.956\times10^{-3}\\
&E = 2.12\times10^5(1.144 - 4.856\times10^{-4}T)\\
&n = 2.263\\
&Q_c/k = 36739
\end{aligned} \quad (7)$$

$$\begin{aligned}
&t_r = \theta\exp(Q/RT)\\
&\ln\theta = A + B\ln\ln\left(\frac{\sigma^*}{\sigma_h}\right)\\
&A = -34.8 + \tanh\left(\frac{\sigma_h - 200}{50}\right) + C\\
&B = \frac{12}{1.5 + 0.5\tanh\left(\frac{\sigma_h - 200}{50}\right)}\\
&C = -0.5\times\left[1 + \tanh\left(\frac{\sigma_h - 200}{50}\right)\right]\times0.75\times\left[1 + \tanh\left(\frac{\dot{T} - 58}{17}\right)\right]\\
&\sigma^* = 730\\
&Q = 70170\\
&R = 1.986
\end{aligned} \quad (8)$$

.

ε_{ss} is secondary creep strain rate in s^{-1}, σ_{eq} is equivalent stress in *MPa*, T is temperature in K, t_r is creep rupture time in s, σ_h is hoop stress in *MPa*, and T is heating rate in K/s.

Kimura [6] measured steady-state creep strain rate and creep rupture time of T92 at 550 ^{o}C ~ 700 ^{o}C. In this study, steady-state creep strain rate depending on temperature and equivalent stress was modeled at 550 ^{o}C ~ 700 ^{o}C. Steady state creep strain rate suggested by this study is given in following equations:

$$\begin{aligned}
&\dot{\varepsilon}_{ss} = \begin{cases} C\left(\frac{\sigma_{eq}}{\sigma_{0.2}}\right)^n & \left(\frac{\sigma}{\sigma_{0.2}} \ge 0.5\right) \\ C'\left(\frac{\sigma_{eq}}{\sigma_{0.2}}\right)^{n'} & \left(\frac{\sigma}{\sigma_{0.2}} < 0.5\right) \end{cases}\\
&\sigma_{0.2} = -1.4831T + 1569.5\\
&C = -3.616\times10^{-4}T + 0.3658\\
&n = -0.068T + 77.064\\
&C' = \frac{C\times0.5^n}{0.5^{n'}}\\
&n' = 4
\end{aligned} \quad (9)$$

.

ε_{ss} is secondary creep strain rate in hr^{-1}, σ_{eq} is equivalent stress in *MPa*, T is temperature in K. Kimura [6] suggested parameters of Monkman – Grant relationship of T92, which is the relationship between steady-state creep strain rate and creep rupture time. Monkman – Grant equation of T92 is suggested in following equation:

$$\ln t_r = -\frac{1}{1.141}\ln\left(\frac{\dot{\varepsilon}_{ss}}{0.0825}\right) \quad (10)$$

t_r is creep rupture time in hr, and ε_{ss} is secondary creep strain rate in s^{-1}.

3.3. *Steady-state operating condition*

Steady-state operating condition of PGSFR is given in Table II.

Table II. Steady-state operating condition

Effective full power day	1160 day
Maximum average burnup	6.61 at%
Maximum local peak burnup	10.47 at%
Average linear heat rate	16 kW/m
Local peak linear heat rate	32.43 kW/m
Channel Coolant flow rate	0.0736 kg/s
Coolant inlet temperature	663 K

3.4. *FE analysis procedure*

The first step of the FE analysis is simplified heat transfer analysis to obtain temperature distribution of cladding. A heat transfer analysis option, *HEAT TRANSFER with user subroutines, UMATHT and FILM supported by Abaqus 2016 was used. Constituent redistribution was ignored in this simplified heat transfer analysis. Axial power peaking factor (PPF) was applied. Coolant temperature at each axial location was calculated by using energy balance equation:

$$\dot{Q}_{i\to x} = \dot{m}(h_x - h_i) \quad (11)$$

$\dot{Q}_{i\to x}$ is integral of linear heat rate from coolant inlet, i to position, x. $\dot{m}$ is coolant mass flow rate, h_x is sodium enthalpy at position, x, and h_i is sodium enthalpy at inlet, i. Convective heat transfer coefficient between coolant

and cladding is calculated by using Schad-Modified Correlation [7]:

$$h = \frac{Nu \times k_{Na}}{D_h}$$

$$Nu = [-16.15 + 24.96(\frac{P}{D}) - 8.55(\frac{P}{D})^2]Pe^{0.3}$$

$$Pe = \frac{\dot{m}}{A_f}\frac{c_{p,Na}D_e}{k_{Na}}$$

$$P = 2r_w + 2r_{co}$$

$$D = 2r_{co}$$

$$A_f = \frac{\sqrt{3}}{4}P^2 - \frac{\pi}{2}r_{co}^2 - \frac{\pi}{2}r_w^2$$

$$P_e = \pi r_{co}$$

$$P_w = \pi r_{co} + \pi r_w$$

$$D_h = \frac{4A_f}{P_e}$$

$$D_e = \frac{4A_f}{P_w} \quad (12)$$

h is convective heat transfer coefficient in $W/m^2/K$, k_{Na} is thermal conductivity of sodium in $W/m/K$, $c_{p,Na}$ is specific heat of sodium in $J/kg/K$, $\dot{m}$ is coolant flow rate in kg/s, r_{co} is cladding outer radius, and r_w is wire radius. The equation above can be used in the range of $150 < Pe < 1000$ and $1.1 < P/D < 1.5$. Thermal boundary condition is suggested schematically in Fig. 2.

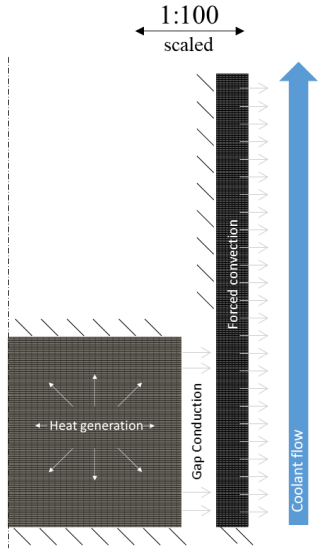

Fig. 2. Thermal boundary condition for heat transfer analysis

The second step of the analysis is structural analysis that considers only cladding part. A transient static structural analysis option, *VISCO with user subroutines, DLOAD, CREEP, and UEXPAN supported by Abaqus 2016 was used. Temperature distribution of the cladding derived from heat transfer analysis was imported. Plenum pressure was linearly increased from 0 MPa to 6.68 MPa. Channel pressure was 0.1 MPa. Boundary condition for structural analysis is suggested schematically in Fig. 3.

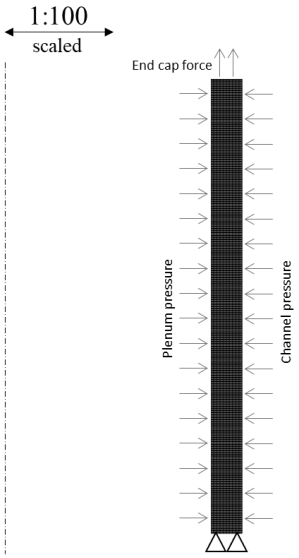

Fig. 3. Boundary condition for structural analysis

3.5. *CDF evaluation*

CDF was calculated in each structural analysis steps. Linear time fraction rule given in following equation was used:

$$CDF = \sum \frac{\Delta t}{t_r}$$

Δt is time increment and t_r is creep rupture time.

4. Results

Temperature distribution of inner and outer cladding on 1160 day calculated by the FE analysis is given in Fig. 4 with the temperature distribution calculated by FEAST-M code [8]. Near the inner surface of cladding, temperature distribution evaluated by FE analysis is overall higher than that by FEAST-M code. The error between the temperature distributions evaluated by the FE analysis and FEAST-M code arises from simplified thermal boundary condition of the FE analysis. Fig. 2 shows the thermal boundary condition of the FE analysis. In the FE analysis, only the gap conduction via sodium is considered. It causes underestimation of heat transfer from fuel to coolant channel, so that the temperature of the cladding increases.

Stress distribution of inner and outer cladding on 1160 day is suggested in Fig. 5. HT9 and T92 claddings are on almost equal stress state. It means that difference of creep strain rate has little effect on stress state of cladding. The radial and axial gradients of stress in Fig. 5 are mainly caused by temperature gradient causing ununiform thermal expansion.

CDF distribution of inner and outer cladding on 1160 day is suggested in Fig. 6. The peak points are not

located on both maximum stress point and maximum temperature point. CDF value of T92 cladding is 10^5 ~ 10^6 times lower than that of HT9 cladding. For most of operating time, the CDF values of the peak points on outer surface are larger than those on inner surface. However, the increase rate of CDF on inner surface becomes faster over time.

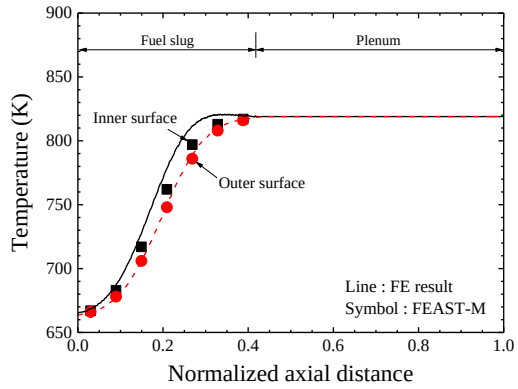

Fig. 4. Temperature distribution of cladding

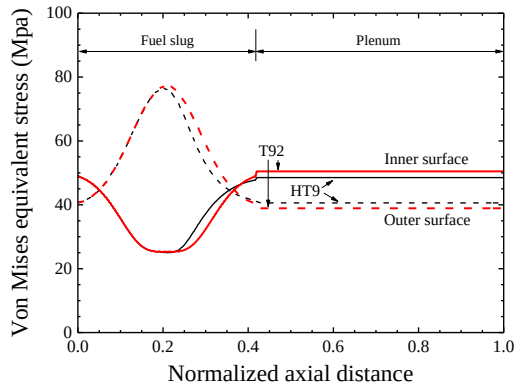

Fig. 5. Stress distribution of cladding

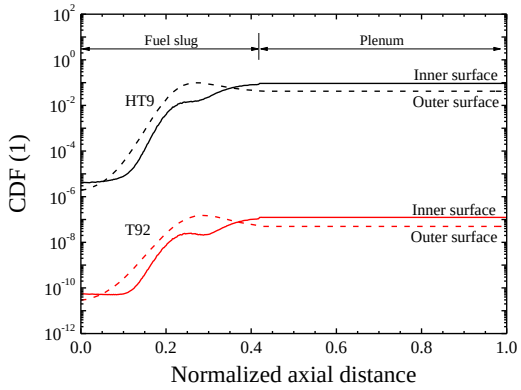

Fig. 6. CDF distribution of cladding

5. Conclusions

In this study, cumulative damage fraction of T92 cladding for the steady-state condition in PGSFR was evaluated. The CDF value of T92 cladding was compared quantitatively with that of HT9 cladding. Through this study, following conclusions were derived:

(1) The difference of creep strain rate between T92 and HT9 has little effect on stress state of cladding. It implies that the difference of creep strain rate between F-M cladding materials is not major factor of calculating CDF.

(2) CDF value of T92 cladding is 10^5 ~ 10^6 times lower than that of HT9. It quantitatively verifies that T92 cladding has much better creep rupture resistance for the steady-state condition than HT9 cladding.

(3) For most of operating time, the CDF values of the peak points on outer surface are larger than those on inner surface. However, the increase rate of CDF on inner surface becomes faster over time. It makes uncertainty of predicting the location of creep rupture of cladding.

In further study, CDF of T92 for transient condition in PGSFR will be evaluated.

ACKNOWLEDGMENT

This research was supported by the National Research Foundation of Korea (NRF) funded by the Ministry of Science and ICT. (NRF-2013M2B2B1075733).

REFERENCES

[1] G. L. Hofman, L. Leibowitz, J. M. Kramer, M. C. Billone and J. F. Koenig, Metallic fuels handbook (No. ANL-IFR—29), Argonne National Laboratory, 1985.
[2] The SAS4A/SASSYS-1 Safety Analysis Code System (No. ANL/NE-16/19), Argonne National Laboratory, 2017.
[3] L. Letibowitz, and R. A. Blomquist, Thermal conductivity and thermal expansion of stainless steels D9 and HT9, International Journal of Thermophysics, Vol. 9, pp. 873-883, 1988.
[4] N. Yamanouchi, M. Tamura, H. Hayakawa, A. Hishinuma, and T. Kondo. Accumulation of engineering data for practical use of reduced activation ferritic steel: 8%Cr 2%W 0.2%V 0.04%Ta Fe, Journal of Nuclear Materials, Vol. 191, pp. 822-826, 1992.
[5] S. Sharafat, R. Amodeo, and N. M. Ghoniem, Material data base and design equations for the UCLA solid breeder blanket (No. UCLA-ENG-8611:PPG-937), California University, 1986.
[6] K. Kimura, K. Sawada, H. Kushima, K. Kubo, Effect of stress on the creep deformation of ASME Grade P92/T92 steels, International Journal of Materials Research, Vol. 99, No. 4, pp. 395-401, 2008.
[7] N. E. Toredas, M. S. Kazimi, Nuclear systems: thermal hydraulic fundamentals, CRC press, 2012.
[8] A. Karahan, Modeling of thermos-mechanical and irradiation behavior of metallic and oxide fuels for sodium fast reactors (Doctoral thesis), Massachusetts Institute of Technology, 2007.